^{7}Li NMR studies on the triangular lattice system LiCrO$_2$

L. K. Alexander,[1] N. Büttgen,[2] R. Nath,[2] A. V. Mahajan,[1] and A. Loidl[2]

[1]*Department of Physics, Indian Institute of Technology, Mumbai 400076, India*

[2]*Experimentalphysik V, Elektronische Korrelationen und Magnetismus, Institut für Physik, Universität Augsburg,*
D-86135 Augsburg, Germany

We report ^{7}Li NMR, magnetic susceptibility, and heat capacity measurements on the triangular lattice Heisenberg antiferromagnet compound LiCrO$_2$. We find that in contrast to NaCrO$_2$, magnetic properties of LiCrO$_2$ have a more pronounced three dimensional character with sharp anomalies in the temperature variation of the ^{7}Li NMR intensity and the NMR spin-lattice relaxation rate $1/T_1$. From heat capacity measurements we find that the total entropy related to the magnetic transition is in agreement with expectations. However, we find a significant contribution to the magnetic entropy in the range from the ordering temperature T_N to nearly $4T_N$. This suggests the existence of magnetic correlations at temperatures well above T_N which might be due to the frustrated nature of the system. Based on the temperature dependence of $1/T_1$, we discuss the possible occurrence of a Kosterlitz-Thouless-Berezinskii (KTB) transition taking place at $T_{KTB}=54$ K in LiCrO$_2$. Heat capacity data at low temperatures ($T \ll T_N$) exhibited a T^3 dependence and the ratio of interlayer to intralayer coupling constants, $J_\perp/J$ in LiCrO$_2$ was found to be $\sim 10^{-3}$. Lithium depletion has no significant effect on the magnetic properties and the behavior of Li$_{0.5}$CrO$_2$ is nearly unchanged from that of LiCrO$_2$.

PACS number(s): 74.25.Ha, 76.60.$-$k, 75.40.Cx, 75.40.$-$s

I. INTRODUCTION

Geometrically frustrated systems are being widely studied due to the possibility of unconventional ground states and their susceptibility to weak perturbations. The two-dimensional triangular lattice Heisenberg antiferromagnet (TLHAF) is a prominent example where exotic magnetic phenomena have been observed. Specifically, while Na$_x$CoO$_2 \cdot 1.3$H$_2$O is superconducting ($0.25 < x < 0.33$), the unhydrated Na$_x$CoO$_2$ also shows a gamut of magnetic transitions.[1–3] Presumably with the above background, Olariu *et al.*[4] investigated NaCrO$_2$ by nuclear magnetic resonance (NMR) and muon spin resonance (μSR) experiments (in addition to bulk probes) and thereby concluded to have observed an extended fluctuating regime in TLHAF. Recent reports on NiGa$_2$S$_4$ (Ref. 5) suggest an unconventional magnetic ground state originating from magnetic correlations which extend beyond nearest neighbors.

In this paper we present a ^{7}Li NMR study of LiCrO$_2$. Supplementary bulk magnetic susceptibility and heat capacity data are also presented. Further, in view of the important role played by the content of sodium in Na$_x$CoO$_2$, measurements on the delithiated compound Li$_{0.5}$CrO$_2$ are also presented. Previous work on LiCrO$_2$ has established that it possesses α-NaFeO$_2$-type structure comprising two-dimensional triangular chromium layers.[6] Magnetic susceptibility data[6,7] indicate a transition at around 62 K. Published susceptibility data could be fitted with a Curie-Weiss law only above 450 K and the paramagnetic Curie temperature is reported in the range 570–700 K.[6–8] Neutron scattering and Raman scattering studies[9–11] suggest a three-dimensional character of the magnetic correlations below the transition temperature (T_N). Above T_N, measurements indicate a wide region showing short-range magnetic correlations.[8] There are no NMR studies or specific heat measurements reported on the compound to date.

Herein, we report ^{7}Li NMR studies, bulk susceptibility, and specific heat measurements carried out on Li$_x$CrO$_2$ ($x = 0.5, 1$). We found that the ^{7}Li NMR spectral intensity of the title compounds drops precipitously at T_N unlike in NaCrO$_2$ where the intensity drops progressively in a 10 K range below T_N. The extended fluctuating regime observed below T_N in NaCrO$_2$ does not appear pronounced in LiCrO$_2$. Our heat capacity measurements exhibit a peak at the magnetic ordering temperature. Both NMR and specific heat studies suggest that magnetic correlations develop well above T_N. The rest of the paper is organized as follows. Section II contains the experimental details, wherein synthesis and structural characterization of Li$_x$CrO$_2$, experimental setup, and parameters for various other measurements such as bulk magnetic susceptibility, specific heat, and NMR are included. In Sec. III, we present the results of our measurements which is followed by a comprehensive discussion in Sec. IV.

II. EXPERIMENTAL DETAILS

Polycrystalline LiCrO$_2$ was synthesized by solid-state reaction of a stoichiometric mixture of Li$_2$CO$_3$ (Aldrich, 99.99%) and Cr$_2$O$_3$ (Aldrich, 98.0%). The mixture was fired at 800 °C for 48 h with one intermediate grinding. X-ray diffraction experiment was carried out using PANalytical X'pert PRO powder diffractometer with X'celerator detector. The diffractometer uses a Cu $K\alpha$ target ($\lambda_{av} = 1.541\,82$ Å). Our results [see Fig. 1(a)] indicate single phase formation and the peaks can be indexed using the trigonal space group, $R\bar{3}m$. Using a least-squares method, the lattice parameters were found to be $a = 2.8949(12)$ Å, $b = 2.8949(12)$ Å, and $c = 14.3886(98)$ Å. As shown in a sketch of the LiCrO$_2$ crystal structure (Fig. 2), Cr layers have a triangular configuration. In the structure, oxygen ions form *ABCABC* type of stacking layers. Also, the edge shared Cr octahedral layers are sepa-
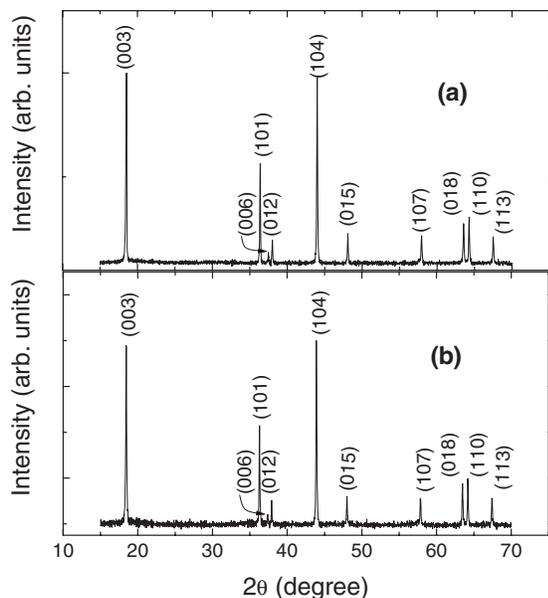
FIG. 1. XRD patterns of (a) $LiCrO_2$ and (b) $Li_{0.5}CrO_2$. Both the peak sets could be completely indexed using the space group $R\bar{3}m$.

rated by Li ions. Each Li has six nearest neighbor oxygen atoms (three above and three below) each of which have three nearest neighbor Cr atoms. Therefore, for a supertransferred hyperfine interaction (mediated by oxygen), Li will feel the effect of 18 Cr spins (nine above and nine below). The crystal structure makes a strong case for two-dimensional (2D) triangular lattice Heisenberg antiferromagnets.

$Li_{0.5}CrO_2$ was prepared by extraction of lithium from $LiCrO_2$ using chemical methods.[12] The extraction was carried out by stirring $LiCrO_2$ powders in an aqueous solution of an oxidizing agent, $Na_2S_2O_8$ (Thomas Baker, 99.0%) for two days with help of a magnetic stirrer. The amount of $Na_2S_2O_8$ required for the delithiation reaction was decided based on our experience with $LiCoO_2$.[13] The delithiation reaction for synthesis of $Li_{0.5}CrO_2$ can be summed up as

$$2LiCrO_2 + 0.5Na_2S_2O_8 \rightarrow 2Li_{0.5}CrO_2 + 0.5Na_2SO_4$$
$$+ 0.5Li_2SO_4.$$
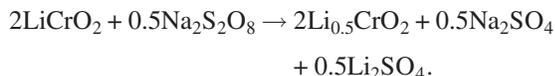
The product was filtered, washed repeatedly—first with water and finally with acetone, and air dried. In order to estimate the level of delithiation in $LiCrO_2$, ^7Li NMR spectral intensities were compared. Here, the NMR spectra were measured in the undelithiated and the delithiated samples under identical conditions and normalized by the respective sample masses. Based on this, $Li_{0.5}CrO_2$ should be written as $Li_{(0.51\pm0.02)}CrO_2$. X-ray diffraction (XRD) pattern of $Li_{0.5}CrO_2$ was found to match exactly with that of $LiCrO_2$ [Fig. 1(b)]. Lattice parameters of $Li_{0.5}CrO_2$ do not vary significantly from those of $LiCrO_2$ quoted in the above paragraph.

Macroscopic magnetic properties were measured using a superconducting quantum interference device magnetometer (MPMS5, Quantum Design) and a vibrating sample magne-
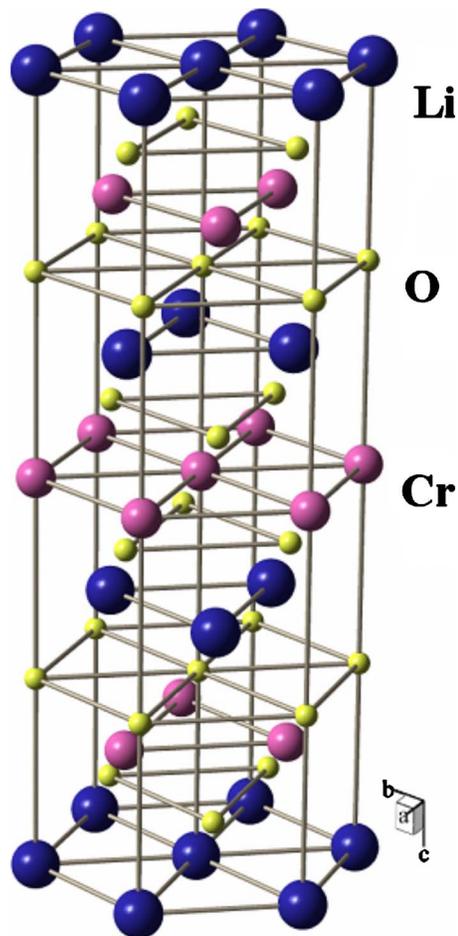
FIG. 2. (Color online) A schematic of the crystal structure of $LiCrO_2$.

tometer (VSM) from Quantum Design. Magnetization (M) was measured as a function of temperature (T) in an applied field (H) of 10 kG and in a temperature range 2–300 K. The M-H isotherms were measured at 280, 200, 150, and 50 K. None of these M-H plots (not shown) exhibited any signs of hysteresis. Also M-H plots at all the temperatures showed a strictly linear field dependence. Ferromagnetic impurities estimated using the plots were found to be negligible. Zero-field-cooled (ZFC) and field-cooled (FC) magnetization measurements were carried out on both the samples. In this experiment, sample was first cooled in zero applied field to 2 K and then the measurements were taken from 2 to 300 K in a field of 50 G (ZFC data). Whereas for the FC measurements, sample was cooled in an applied field of 50 G. Then in the same field, data were collected in the temperature range $2 < T < 300$ K.

Solid-state NMR is an efficient local probe of magnetic properties. This technique allows one to study static magnetic correlations and low-energy spin excitations. Our NMR experiments were carried out using a homebuilt NMR spectrometer. We used an Oxford Instruments (sweepable) superconducting magnet and a variable temperature insert. In the experiments, ^7Li nuclei (nuclear spin $I=3/2$ and gyromagnetic ratio $\gamma/2\pi=16.546$ MHz/T) were probed using pulsed
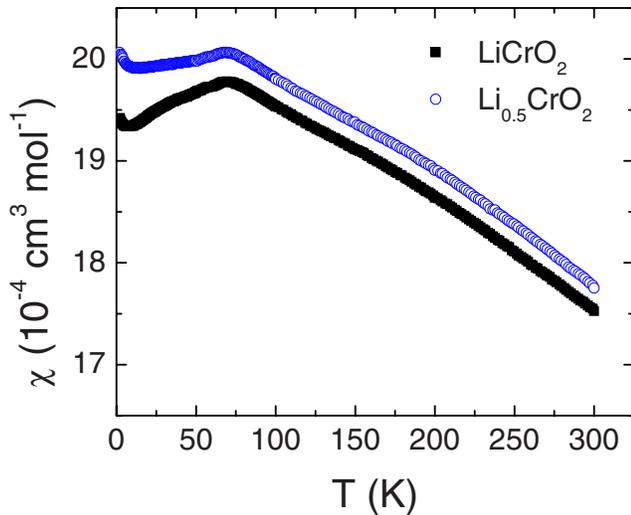
FIG. 3. (Color online) Temperature dependence of bulk magnetic susceptibility (M/H) of $LiCrO_2$ and $Li_{0.5}CrO_2$ in an applied field of 1 T between 2 and 300 K.

NMR technique. Measurements were carried out in the temperature range $2 < T < 300$ K. Spectra were obtained employing fast Fourier transform (FFT) technique at a fixed field of 10.89 kG. At low temperatures (below 10 K), since the spectra were too broad for an accurate FFT experiment, field sweep measurement at a frequency of 18 MHz was carried out to supplement the spectral data. In order to check the field dependence for the NMR characteristics of the compound, measurement was also done at a higher applied field by sweeping the field at 71 MHz (applied field $H \approx 43$ kG). It also allows us to investigate the field dependence of the extended fluctuation regime, if any. An aqueous solution of LiCl was used as the diamagnetic reference. NMR spin echoes were obtained using $\pi/2 - \tau - \pi$ pulse sequences. At 18 MHz, $\pi/2$ pulse widths were typically in the range $1 - 8$ μs for $LiCrO_2$ and $Li_{0.5}CrO_2$. At 71 MHz, typical $\pi/2$ pulse widths were 4 μs. For spin-lattice relaxation measurements, the inversion-recovery method was employed. The spin-spin relaxation rate ($1/T_2$) was determined by measuring the decay of echo intensity as a function of the separation between the $\pi/2$ and π pulse.

Specific heat measurements were carried out on $LiCrO_2$ in the temperature range $3 - 300$ K using a Quantum Design PPMS system. $LiCoO_2$ is a nonmagnetic equivalent[13] of $LiCrO_2$ having the same crystal structure. Therefore, in order to extract the magnetic part of the specific heat of $LiCrO_2$, isostructural $LiCoO_2$ was measured. For this purpose, $LiCoO_2$ was prepared as reported elsewhere.[13]

III. RESULTS

A. Bulk magnetic susceptibility

The temperature dependence of bulk magnetic susceptibility $\chi(T)(=M/H)$ for both $LiCrO_2$ and $Li_{0.5}CrO_2$ is shown in Fig. 3. In both the samples, one can see that $\chi(T)$ increases with decreasing temperature until a broad maximum is
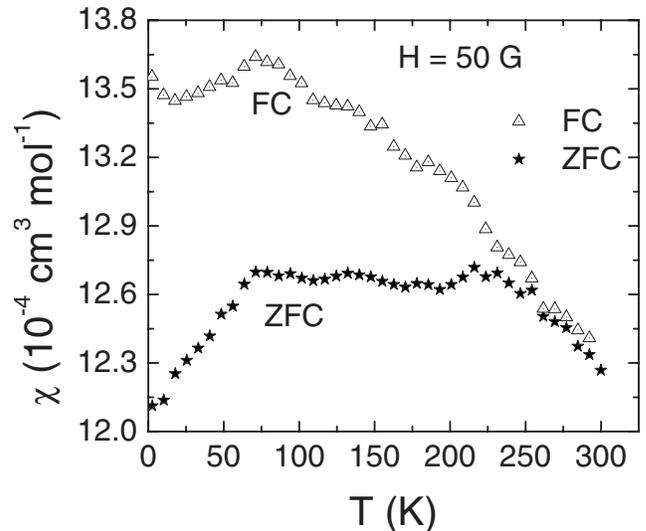
FIG. 4. Zero-field-cooled (ZFC) and field-cooled (FC) magnetic susceptibilities for $LiCrO_2$ as a function of temperature between 2 and 300 K in a field of 50 G. The plot shows a clear splitting of the ZFC and FC curves. The scatter in the data is due to the small magnetization produced by a 50 G field which is near the limiting sensitivity of the VSM.

reached at about 62 K and below this temperature $\chi(T)$ is nearly constant. In line with the reported results,[6–8] we found that the susceptibility data of $LiCrO_2$ do not obey the Curie-Weiss law below 300 K. A negligible low-temperature Curie tail implies the presence of very low amounts of paramagnetic impurities and the high quality of our samples. The anomaly at 62 K in $LiCrO_2$ has been associated with antiferromagnetic (AF) order.[9,10] A nearly constant (but somewhat higher) value of susceptibility for $Li_{0.5}CrO_2$ compared to $LiCrO_2$ through the entire temperature region measured and a slightly enhanced low-temperature Curie tail appears to indicate that delithiation has generated small amounts of paramagnetic impurities which remained even after repeated washing. Figure 4 shows ZFC and FC magnetization data for $LiCrO_2$. There, one observes a splitting of the ZFC and FC curves at around 240 K. This history dependent magnetization for $LiCrO_2$ has not been reported until now. In the case of $Li_{0.5}CrO_2$, as well, we observed roughly the same features as that of $LiCrO_2$. We checked for the possible origin of this ZFC-FC splitting from any unnoticed impurities (in spite of the negligible Curie tail, and the single phase x-ray diffraction spectrum), especially oxides of chromium. CrO_2 has a ferromagnetic transition temperature of 400 K. Cr_2O_3 and Cr_2O_5 have antiferromagnetic transitions at 307 and 125 K, respectively. An intrinsic reason for the history dependent magnetization observed in Li_xCrO_2 is then indicated. However, keeping in mind that the effect observed is small, other explanations might be possible.

B. NMR measurements

1. Spectra

As seen in Fig. 2, the Li nuclei can have a hyperfine coupling (presumably via the oxygen ions) with the magnetic
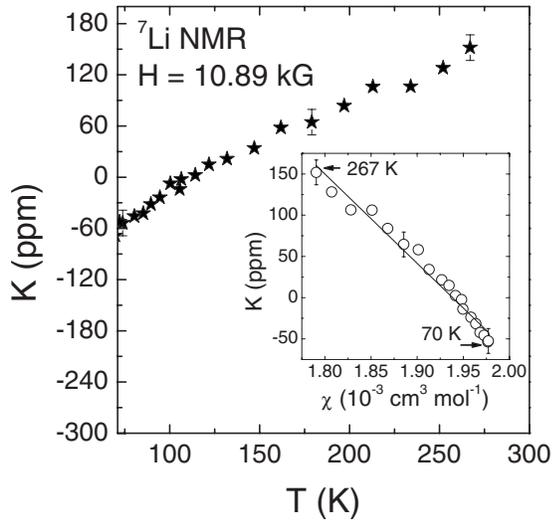
FIG. 5. Variation of ^{7}Li NMR shift, $K(T)$ with temperature for LiCrO$_2$ above the region of transition temperature. The inset shows plot of K versus bulk susceptibility, χ with temperature as an implicit parameter. From this plot, using Eq. (1), hyperfine coupling field was estimated to be around 6 kG.

Cr^{3+} ions which are present in triangular planes above and below the Li planes. The spin susceptibility of the Cr^{3+} ions $\chi_{spin}(T)$ gives rise to a shift of the ^{7}Li resonance $K(T)$ following

$$N_A \mu_B K(T) = H_{hf} \chi_{spin}(T), \qquad (1)$$

where N_A is the Avogadro number, μ_B is the Bohr magneton, and H_{hf} is the hyperfine field. In both LiCrO$_2$ and Li$_{0.5}$CrO$_2$ at both the frequencies, 18 and 71 MHz, we found that the spectra have a small temperature dependence of the shift. This nature of variation is expected since the absolute variation of the susceptibility from 300 to 60 K is itself very small. Figure 5 shows variation of NMR shift with temperature for LiCrO$_2$ above the region of the transition temperature. The inset shows a plot of K versus bulk susceptibility χ with temperature as an implicit parameter. From this plot, using Eq. (1), the hyperfine field H_{hf} was estimated to be 6 ± 1 kG. This result suggests a weak hyperfine coupling between Li and Cr. This is in agreement with the results on NaCrO$_2$ (Ref. 4).

Figure 6 shows the spectra of LiCrO$_2$ in the region of transition. Integrated spectral intensity, which is proportional to the number of ^{7}Li nuclei, is roughly constant above 70 K. At around 62 K, intensity falls sharply—as also shown in Fig. 7 (corrected for temperature and T_2 effects). This sharp decline indicates the onset of long-range order. The signal disappears completely at around 55 K. In a conventional case, the spectra broaden as one approaches the ordering temperature from above and eventually disappear (from the window of observation) below the ordering temperature due to the large static field that develops in the ordered state. Here in LiCrO$_2$ at 10 kG, the ^{7}Li NMR signal reappeared at around 35 K. By around 12 K, a small signal could be observed but the spectrum was too broad to reliably obtain the
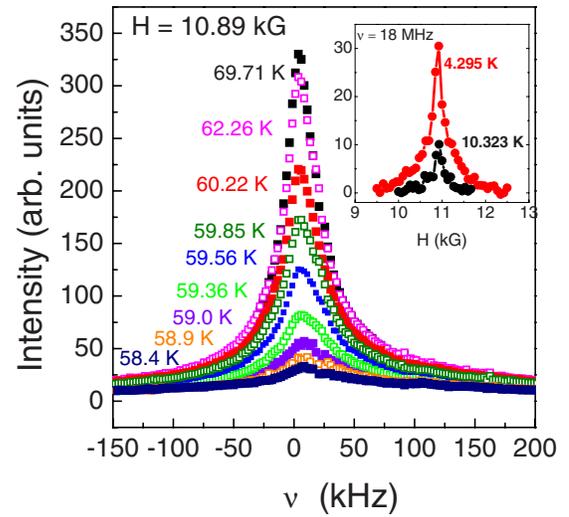
FIG. 6. (Color online) ^{7}Li NMR FFT spectra of LiCrO$_2$ in the region of transition. The inset shows field sweep spectra at low temperatures of 10 and 4 K.

line shape using FFT techniques. Therefore, in Fig. 7, data shown below 10 K were taken by sweeping the field at 18 MHz. Resultant spectra are shown in the inset of Fig. 6. Here in LiCrO$_2$, unlike the case of NaCrO$_2$ (Ref. 4), intensity is not regained completely down to 4 K. Spectra of Li$_{0.5}$CrO$_2$ also showed a similar temperature dependence.

Spectra of LiCrO$_2$ in an applied field of $H \approx 43$ kG showed a qualitatively similar behavior with small differ-
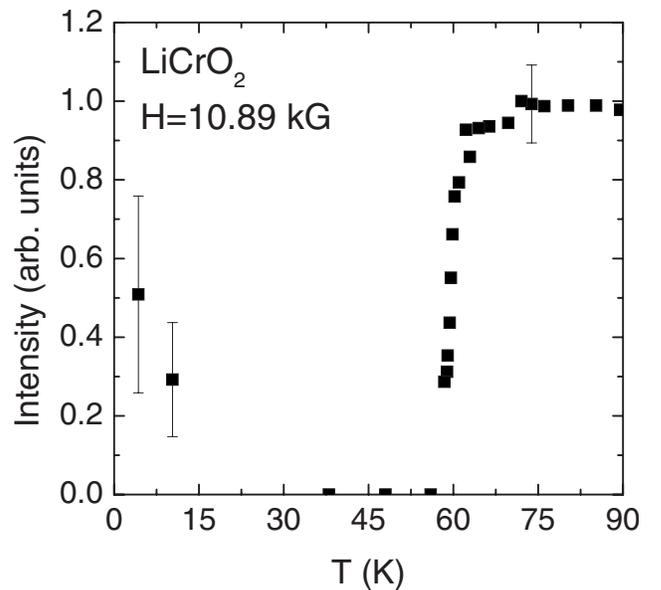
FIG. 7. Temperature dependence of the ^{7}Li NMR spectral intensity of LiCrO$_2$ obtained at 18 MHz between 4 and 90 K. Here, echo integrated intensities have been corrected for temperature and T_2 effects. The error bar shown at 73 K is exemplary and indicates the value of error common to all the data points shown above 58 K. NMR signal was completely absent from 56 to 35 K. The low-temperature points at 10 and 4 k were obtained from the field sweep spectra (cf. the inset of Fig. 6).
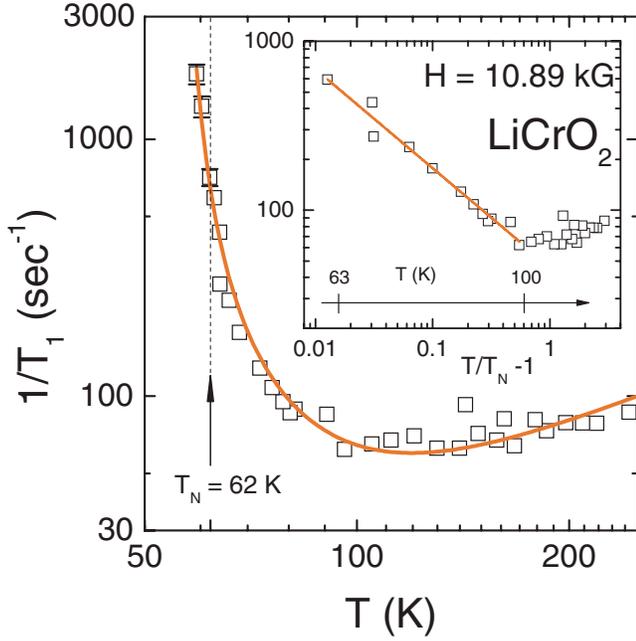
FIG. 8. (Color online) Temperature dependence of ^{7}Li NMR spin-lattice relaxation rate, $1/T_1$ for LiCrO$_2$ at H=10.89 kG. The solid line shown in the plot is fit of the relaxation data with Eq. (3) (discussed in Sec. IV). Inset: Logarithmic plot of the $1/T_1$ vs (T/T_N-1).

ences. The intensity sharply falls at around 62 K and continues to fall until about 52 K. The signal is never completely lost and about 30% of the signal is regained by about 8 K.

2. Spin-lattice relaxation rate $1/T_1$

In LiCrO$_2$ and Li$_{0.5}$CrO$_2$, for 18 and 71 MHz (corresponding fields around 10 and 43 kG, respectively), the recovery of the nuclear magnetization after an inverting pulse was single exponential. The recovery data fitted well to the expression

$$\left[\frac{M(t)-M_\infty}{2M_\infty}\right] = Ae^{(-t/T_1)} + C, \qquad (2)$$

where $M(t)$ is the nuclear magnetization at a time t after an inverting pulse and M_∞ is the equilibrium value of the magnetization.[14] Temperature dependence of $1/T_1$ for H =10.89 kG for LiCrO$_2$ is presented in Fig. 8. In LiCrO$_2$, the spin-lattice relaxation rate shows a divergence around 62 K due to slowing down of fluctuations as one approaches magnetic order. This is around the same temperature at which a broad maximum in the bulk susceptibility $\chi(T)$ was observed, accompanied by an intensity loss of the NMR spectra. Below 59 K, the [7]Li signal was very weak and broad and did not allow for complete saturation for accurate relaxation rate measurements.

At 71 MHz ($H \approx 43$ kG), relaxation rates were measured between 250 and 80 K. The results (not shown) were in reasonable agreement with those at 18 MHz. Measurements on Li$_{0.5}$CrO$_2$ at 18 MHz gave results similar to those on LiCrO$_2$.
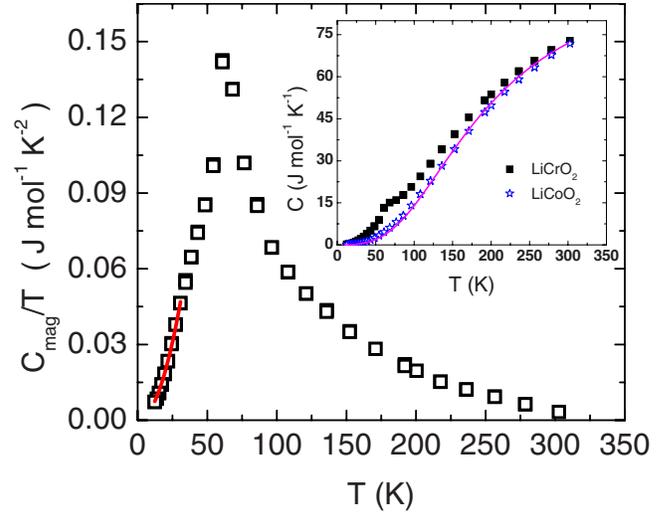
FIG. 9. (Color online) Variation of magnetic specific heat divided by temperature (C_{mag}/T) for LiCrO$_2$. C_{mag} was obtained by subtracting the specific heat of nonmagnetic LiCoO$_2$ (see text). The solid line at $T < 30$ K shows fit of the C_{mag}/T data with Eq. (9) (discussed in Sec. IV). Inset: Specific heat capacity versus temperature for LiCrO$_2$ and LiCoO$_2$. The solid line shows fit of the LiCoO$_2$ heat capacity data with Eq. (7) (discussed in Sec. IV).

C. Specific heat capacity

Results of the specific heat measurements are shown in Fig. 9. The inset shows the temperature dependence of specific heat capacity of LiCrO$_2$ and LiCoO$_2$. Layered LiCoO$_2$ is nonmagnetic and isostructural with LiCrO$_2$. Also, in a Debye model picture, the Debye temperatures of the two compounds are expected to be nearly the same taking into account their molecular weights and unit cell volumes.[15] Indeed, at high temperatures, the heat capacities of the two compounds coincide. Therefore, magnetic contribution to the measured specific heat of LiCrO$_2$ (C_{mag}) is determined by direct subtraction of the measured specific heat of LiCoO$_2$ from that of LiCrO$_2$. C_{mag}/T shows a peak at around 62 K, in good agreement with anomalies observed by us in bulk magnetic susceptibility and NMR measurements.

IV. DISCUSSION

The magnetic susceptibility of LiCrO$_2$ has been reported by several groups.[6–8] The main conclusion has been that a Curie-Weiss behavior (indicative of noninteracting local moments) is valid only above about 400 K. A large range from 400 to 62 K (at which long-range order finally sets in) in which magnetic correlations are present is probably due to the frustrating magnetic interactions of the triangular Cr planes.

We found that delithiation of LiCrO$_2$ did not have a significant impact on its magnetic properties. This is quite unlike the case of NaCoO$_2$ where the magnetic ground state depends strongly on the Na content. This implies that the smaller Li ion does not impact the magnetism of the Cr layers nor does it contribute mobile charge carriers in the planes.

As seen from the structure, each Li has a supertransferred hyperfine coupling to the Cr layers via oxygen ions. Since six Cr ions (three ions from three triangles of which three ions are common) from each layer might be expected to affect each Li, the Li senses a distribution of susceptibilities and hence a linewidth which increases with decreasing temperature as also with increasing field. In the ordered state, a 120° alignment of the spins on the vertices of the triangles will give a cancellation of hyperfine fields at the Li site. The linewidth might remain large due to any structural and magnetic disorder. In the case of $NaCrO_2$, an extended fluctuating regime was reported below T_N and the full NMR signal intensity was recovered by about 10 K. While Olariu *et al.*[4] did not show NMR $1/T_1$ data for $NaCrO_2$, their relaxation rate data from μSR showed a peak at 30 K which is much lower than the ordering temperature of 40 K in that compound. They therefore concluded that an extended fluctuating regime exists for $NaCrO_2$ below its T_N. On the other hand, our ^{7}Li NMR spin-lattice relaxation rate for $LiCrO_2$ diverges at T_N. This indicates a stronger interplane interaction in $LiCrO_2$ compared to $NaCrO_2$. The divergence of the spin-lattice relaxation rate $1/T_1(T)$ in $LiCrO_2$ is indicated by the inset of Fig. 8, where we plot logarithmically $1/T_1$ versus the reduced temperature $T/T_N - 1$. It demonstrates that the critical temperature dependence of $1/T_1(T)$ with a power law extends far beyond the critical region near T_N which evokes another mechanism to be describe the nuclear spin-lattice relaxation rate.

Theoretical study by Kawamura and Miyashita[16] have suggested the occurrence of Kosterlitz-Thouless-Berezinskii (KTB) type of phase transition[17–19] in 2D triangular lattice antiferromagnets, complemented by the inherent frustration effects. Here, the correlation between the spins generates vortices which stay as bounded pairs at low temperatures. But at a critical temperature, T_{KTB} ($\neq 0$), these bounded vortex-antivortex pairs dissociate to free vortices resulting in a topological phase transition. Spin-lattice relaxation measurements can provide clues for the order driven by the free vortices at temperatures above T_{KTB} in 2D antiferromagnets.[20,21] For $T > T_{KTB}$, spin-lattice relaxation rate $1/T_1$ has two contributions: The first due to free vortices and the second due to spin-wave excitations, as given in the equation below.

$$\frac{1}{T_1} = \alpha \left(\frac{\gamma g H_{hf}}{z'} \right)^2 \frac{z'}{\sqrt{\pi \cdot n_v U}} + \beta T, \qquad (3)$$

where α is a prefactor, H_{hf} is the hyperfine field, γ is the gyromagnetic ratio for ^{7}Li nucleus, $z' = 18$ is the number of local moments interacting with the probing nuclei and corresponding to a 2D correlation length ξ, and $n_v = 1/(2\xi)^2$ is the density of free vortices,[22]

$$n_v = \left(\frac{1}{2\xi_0} \right)^2 \exp\left(\frac{-2b}{\sqrt{\tau}} \right), \qquad (4)$$

where $\tau = T/T_{KTB} - 1$ and $\xi_0 \simeq a$, the lattice parameter, and b is a scaling parameter. The ideal value for b is $\pi/2$, but theoretical calculation and later experimental reports[20,21,23] allow for smaller values. Free vortices move through the

lattice inducing spin flipping and the vortex velocity U (Ref. 24) is given by

$$U = \left[\frac{\pi}{2} \left(\frac{JS^2 a^2}{\hbar} \right)^2 n_v \ln \frac{k_B T_{KTB}}{JS^2 n_v a^2} \right]^{1/2}. \qquad (5)$$

The solid line in Fig. 8 shows fit of Eq. (3) to our $1/T_1(T)$ data, with $H_{hf} = 6$ kG [from the K vs χ plot (Fig. 5)], Landé factor $g = 1.98$ (based on reports of electron paramagnetic resonant (EPR) measurements by Moreno *et al.*[8]), $J/k_B = 80$ K (Ref. 25), and four free parameters α, β, b, and T_{KTB}. The corresponding T_{KTB} for $LiCrO_2$ was found to be 54 K which is close to the value obtained by Ajiro *et al.*[26] of 60 K and might explain the temperature dependence of the spin-lattice relaxation rate above T_N. A smaller prefactor $\alpha = 0.14 < 1$ than expected ($\alpha = 1$) might arise due to a wave-vector $\vec{q}$ dependence of the hyperfine coupling. For the scaling parameter b, the fit yields the value $b = 0.98$.

The coefficient of the linear term in Eq. (3) was found to be $\beta = 0.24$ s^{-1} K^{-1}. As mentioned earlier, the linear increase in $1/T_1$ data at temperatures above 120 K can be attributed to spin-wave excitations. Such behavior has also been observed in another 2D system $BaNi_2(PO_4)_2$.[20] However, considering the limited temperature range of our data, it is possible to model the data without the spin-wave contribution. In the paramagnetic (high temperature) limit, one expects the relaxation rate value to level off as the fluctuations of local moments are fast and random. In a case where the nuclear relaxation mechanism is mainly governed by fluctuations of localized spins, $1/T_1(T)$ in the high temperature limit, $1/T_{1\infty}$ is given by[27,28]

$$\frac{1}{T_{1\infty}} = \sqrt{2\pi} \left(\frac{\gamma g H_{hf}}{z'} \right)^2 \frac{z' S(S+1)}{3\omega_{ex}}, \qquad (6)$$

where ω_{ex} is the exchange frequency of local moments given by $\omega_{ex} = k_B |\theta_{cw}| / [\hbar \sqrt{zS(S+1)/6}]$. z and z' are the number of local moments exchange coupled with each other ($=6$, here) and that of local moments interacting with the probing nuclei ($=18$, here) at nonmagnetic crystal sites, respectively. The other parameters represent usual physical constants. For $LiCrO_2$, $g = 1.98$ was taken from reports of EPR measurements by Moreno *et al.*[8] Thus, using Eq. (6), spin-lattice relaxation rate of $LiCrO_2$ in the paramagnetic region was found to be 64 s^{-1}. This is close to our high temperature spin-lattice relaxation rate.

The heat capacity of nonmagnetic $LiCoO_2$ could be fitted reasonably well in the full temperature range using the Debye model (see inset of Fig. 9) which yields for the specific heat at constant volume C_v,

$$C_v = 9 r N_A k_B \left[\left(\frac{4T^3}{\theta^3} \right) \int_0^{\theta/T} \frac{x^3 dx}{e^x - 1} - \frac{\theta/T}{e^{\theta/T} - 1} \right], \qquad (7)$$

where r is the number of atoms per formula unit, N_A is the Avogadro's number, k_B is the Boltzmann constant, and θ is the Debye temperature. For $LiCoO_2$, the Debye temperature θ was found to be about 800 K.

As mentioned earlier, magnetic contribution to the specific heat of LiCrO$_2$ (C_{mag}) was determined by direct subtraction of the specific heat of LiCoO$_2$ from that of LiCrO$_2$. Now we discuss the temperature dependence of C_{mag} of LiCrO$_2$. Recently Du et al.[29] based on the spin-wave theory calculations have shown that for TLHAF, at low temperatures ($T << T_N$), magnetic contribution to the heat capacity varies with temperature as follows:

$$C_{mag} = N_A k_B \frac{4\pi^2}{15\sqrt{3}(J_\perp/k_B)(J/k_B)^{5/2}S^3} \left\{ \frac{2}{[9/2 + 4(J_\perp/J)]^{3/2}} + \frac{1}{[9 + 4(J_\perp/J)]^{3/2}} \right\} T^3. \quad (8)$$

Here J and $J_\perp$ represent the intralayer and interlayer exchange constants, respectively. This equation is valid specifically for TLHAF with antiferromagnetic intralayer and interlayer interactions. Electronic structure calculations[30] have, in fact, suggested that this scenario is applicable for LiCrO$_2$.

For negligible $J_\perp/J$ and $S = 3/2$, molar magnetic specific heat for LiCrO$_2$ with $J/k_B = 80$ K (Ref. 25) is

$$C_{mag} = \left(\frac{1.6125 \times 10^{-5}}{\sqrt{J_\perp/k_B}} \right) T^3. \quad (9)$$

We found that the low-temperature region of magnetic heat capacity (below 30 K) shows a T^3 dependence (Fig. 9), with a fitting coefficient equal to 5×10^{-5} J mol^{-1} K^{-4}. Using this experimental result and Eq. (9), we obtain the value of interplanar coupling constant, $J_\perp/k_B$ for LiCrO$_2$ to be around 0.104 K, implying $J_\perp/J \sim 10^{-3}$. Electronic structure calculations by Mazin[30] have indeed predicted a "very weak" interplane coupling.

The total entropy related to magnetic order in LiCrO$_2$ can be determined by finding the area under the curve of the C_{mag}/T vs T plot of Fig. 9 ($12 < T < 300$ K). We obtained a value of 12(1) J mol^{-1} K^{-1} for the magnetic entropy S_{mag} which is in reasonable agreement with the expected value $R \ln(2S+1) = 11.53$ J mol^{-1} K^{-1} where R is the gas constant and $S = 3/2$ for Cr^{3+}. Nearly 80% of the contribution to the magnetic entropy change for LiCrO$_2$ comes from temperatures above T_N. This appears similar to the case of NaCrO$_2$ but in contrast to the entropy behavior in conventional long-range ordered materials.

Below 240 K, Li$_x$CrO$_2$ shows a small history dependence (difference between the ZFC and FC susceptibility curves). This ZFC-FC splitting might be connected to the formation of frozen magnetic clusters, which are singular regions with quite local magnetic interactions. Such a history dependence at temperatures much above the transition temperature has been reported earlier in geometrically frustrated compounds

such as Li$_x$Zn$_{1-x}$V$_2$O$_4$ ($0 \leq x \leq 0.9$) (Refs. 31 and 32) and Tb$_2$Mo$_2$O$_7$.[33] Here in LiCrO$_2$, the origin of the clusters may be from the complex intralayer magnetic correlations additionally influenced by the possible presence of free vortices.

The measurements show that LiCrO$_2$ is long-range ordered below 62 K. The bulk magnetic susceptibility, $\chi(T)$, and magnetic specific heat, C_{mag}, suggest the presence of a short-range order in LiCrO$_2$ even at temperatures well above 62 K. Susceptibility data show a relatively weak anomaly at the ordering temperature. NMR spin-lattice relaxation data suggest the presence of free vortices in the lattice above 62 K. From our ⁷Li NMR relaxation rate analysis, based on expectations for a pure Kosterlitz-Thouless-Berezinskii system, we determined $T_{KTB} = 54$ K. In the present system, however, interplane interactions lead to long-range order below 62 K.

V. CONCLUSION

In summary, we have performed ⁷Li NMR, bulk susceptibility, and heat capacity measurements on the TLHAF LiCrO$_2$. Anomalies in the NMR intensity, spin-lattice relaxation rate, bulk susceptibility, and heat capacity indicate an antiferromagnetic ordering temperature (T_N) of about 62 K in LiCrO$_2$. An extended fluctuating regime below T_N appears to be much less prominent in LiCrO$_2$ compared to NaCrO$_2$. The interplanar magnetic interactions, as well, are therefore stronger in LiCrO$_2$ compared to NaCrO$_2$. A significant magnetic contribution to the specific heat exists above T_N. Magnetic susceptibility and specific heat data suggest the presence of a considerable amount of magnetic short-range order even at temperatures well above T_N. This is corroborated by the temperature dependence of the ⁷Li nuclear spin-lattice relaxation rate $1/T_1(T)$ above T_N which was modeled to arise from free moving vortices in the LiCrO$_2$ lattice. Our value of $T_{KTB} = 54$ K is similar to that estimated by Ajiro et al.[26] of 60 K. Heat capacity data at low temperatures ($T << T_N$) exhibited a T^3 dependence and yielded the ratio of interlayer and intralayer coupling constants in LiCrO$_2$, $J_\perp/J$ to be around 10^{-3}. Lithium depletion does not have a significant effect on the magnetic properties of LiCrO$_2$ in contrast to Na depletion in isostructural NaCoO$_2$. More experiments and theoretical investigations on TLHAF's are needed to obtain a full understanding of their static and dynamic magnetic properties.

[1] K. Takada, H. Sakurai, E. Takayama-Muromachi, F. Izumi, R. A. Dilanian, and T. Sasaki, Nature (London) **422**, 53 (2003).

[2] J. Sugiyama, J. H. Brewer, E. J. Ansaldo, H. Itahara, T. Tani, M. Mikami, Y. Mori, T. Sasaki, S. Hébert, and A. Maignan, Phys. Rev. Lett. **92**, 017602 (2004).

[3] M. L. Foo, Y. Wang, S. Watauchi, H. W. Zandbergen, T. He, R. J. Cava, and N. P. Ong, Phys. Rev. Lett. **92**, 247001 (2004).

[4] A. Olariu, P. Mendels, F. Bert, B. G. Ueland, P. Schiffer, R. F. Berger, and R. J. Cava, Phys. Rev. Lett. **97**, 167203 (2006).

[5] S. Nakatsuji, Y. Nambu, H. Tonomura, O. Sakai, S. Jonas, C. Broholm, H. Tsunetsugu, Y. Qiu, and Y. Maeno, Science **309**, 1697 (2005).

[6] A. Tauber, W. M. Moller, and E. Banks, J. Solid State Chem. **4**, 138 (1972).

[7] C. Delmas, G. Le Flem, C. Fouassier, and P. Hagenmuller, J. Phys. Chem. Solids **39**, 55 (1978).

[8] N. O. Moreno, C. Israel, P. G. Pagliuso, A. J. Garcia-Adeva, C. Rettori, J. L. Sarraoa, J. D. Thompson, and S. B. Oseroff, J. Magn. Magn. Mater. **272-276**, 1023(E) (2004).

[9] J. L. Soubeyroux, D. Fruchart, C. Delmas, and G. Le Flem, J. Magn. Magn. Mater. **14**, 159 (1979).

[10] H. Kadowaki, H. Takei, and K. Motoya, J. Phys.: Condens. Matter **7**, 6869 (1995).

[11] M. Suzuki, I. Yamada, H. Kadowaki, and F. Takeif, J. Phys.: Condens. Matter **5**, 4225 (1993).

[12] S. Choi and A. Manthiram, J. Electrochem. Soc. **149**, A162 (2002).

[13] L. K. Alexander, N. Büttgen, A. V. Mahajan, and A. Loidl (unpublished).

[14] The temperature independent constant C is incorporated in Eq. (2) to account for the noise level of the data.

[15] Debye temperature, $\theta \propto 1/(V^{1/3}M^{1/2})$ where V is the volume of the crystal unit cell and M is the molecular mass. Here in our case, higher molecular mass of $LiCoO_2$ is almost neutralized by the bigger volume of $LiCrO_2$ to get an expected ratio of Debye temperatures to be about 1.01.

[16] H. Kawamura and S. Miyashita, J. Phys. Soc. Jpn. **53**, 4138 (1984).

[17] J. M. Kosterlitz and D. J. Thouless, J. Phys. C **6**, 1181 (1973).

[18] J. M. Kosterlitz, J. Phys. C **7**, 1046 (1974).

[19] V. L. Berezinskii, Sov. Phys. JETP **32**, 493 (1971).

[20] P. Gaveau, J. P. Boucher, L. P. Regnault, and Y. Henry, J. Appl. Phys. **69**, 6228 (1991).

[21] F. G. Mertens, A. R. Bishop, G. M. Wysin, and C. Kawabata, Phys. Rev. B **39**, 591 (1989).

[22] D. J. Bishop and J. D. Reppy, Phys. Rev. Lett. **40**, 1727 (1978).

[23] M. Heinrich, H.-A. Krug von Nidda, A. Loidl, N. Rogado, and R. J. Cava, Phys. Rev. Lett. **91**, 137601 (2003).

[24] D. L. Huber, Phys. Rev. B **26**, 3758 (1982).

[25] Whereas Refs. 7 and 11 use the Hamiltonian $-2J\Sigma_{ij}\mathbf{S}_i \cdot \mathbf{S}_j$ and obtain $J/k_B = 40 \pm 2$ K, we use the Hamiltonian $-J\Sigma_{ij}\mathbf{S}_i \cdot \mathbf{S}_j$. Therefore, we use $J/k_B = 80$ K in our analysis.

[26] Y. Ajiro, H. Kikuchi, S. Sugiyama, T. Nakashima, S. Shamoto, N. Nakayama, M. Kiyama, N. Yamamoto, and Y. Oka, J. Phys. Soc. Jpn. **57**, 2268 (1988).

[27] T. Moriya, Prog. Theor. Phys. **16**, 26 (1956).

[28] N. Büttgen, A. Zymara, C. Kegler, V. Tsurkan, and A. Loidl, Phys. Rev. B **73**, 132409 (2006).

[29] A. Du, G. Z. Wei, and J. Li, Phys. Status Solidi B **234**, 636 (2002). Their spin Hamiltonian is $-J\Sigma_{ij}\mathbf{S}_i \cdot \mathbf{S}_j$. Therefore we use $J/k_B = 80$ K.

[30] I. I. Mazin, Phys. Rev. B **75**, 094407 (2007).

[31] M. Reehuis, A. Krimmel, N. Büttgen, A. Loidl, and A. Prokofiev, Eur. Phys. J. B **35**, 311 (2003).

[32] Y. Ueda, N. Fujiwara, and H. Yasuoka, J. Phys. Soc. Jpn. **66**, 778 (1997).

[33] B. D. Gaulin, J. N. Reimers, T. E. Mason, J. E. Greedan, and Z. Tun, Phys. Rev. Lett. **69**, 3244 (1992).